International Journal of Robotics and Control Systems
Vol. 5, No. 4, 2025, pp. 2178-2196
ISSN 2775-2658
http://pubs2.ascee.org/index.php/ijrcs

Optimal Synergetic and Feedback Linearization Controllers Design for Overhead Crane Systems: A Comparative Study

Batool Hussain [a,1,*], Ahmed Ibraheem Abdulkareem [a,2], Huthaifa Al-Khazraji [a,3]

[a] University of Technology-Iraq, Baghdad, Iraq
[1] cse.24.02@grad.uotechnology.edu.iq; [2] 60162@uotechnology.edu.iq; [3] 60141@uotechnology.edu.iq
* Corresponding Author

ARTICLE INFO

Article history
Received August 04, 2025
Revised September 24, 2025
Accepted November 04, 2025

Keywords
Overhead Crane System;
Nonlinear Control;
Synergetic Control;
Lyapunov Function;
Feedback Linearization;
State Feedback Controller;
Flower Pollination Algorithm

ABSTRACT

This study presents a performance comparison between a synergetic controller (SC) and a feedback linearization based state feedback controller (FL-SFC) applied to overhead crane system. At first, the mathematical model of the system is formulated. Thereafter, the design of both SC and FL-SFC are elaborated, leading to the development of control laws for the proposed controllers. For the SC design, the Lyapunov function is employed to guarantee an exponential convergence of the tracking error to zero. In the FL-SFC approach, an equivalent transformation is used to convert the nonlinear system into a linear form, and then the state feedback controller (SFC) method is utilized to make the error function reach zero where accordingly the crane moves to the specified displacement with minimum sway angle. Taking the advantages of simulating the global pollination process, enabling effective exploration of the entire search space and reducing the risk of being trapped in local minima, the flower pollination algorithm (FPA) is used to tune the design variables of the controllers based on the integral absolute error (IAE) criterion. MATLAB software is used to perform the simulation of the two proposed methods into the crane system. The results show that the SC exhibits a good performance in normal operation and a robustness test involving system parameters' changes than the FL-SFC.

© 2025 The Authors.
Published by Association for Scientific Computing Electrical and Engineering.
This is an open-access article under the CC–BY-NC license.

1. Introduction

Overhead crane systems are used in many different industrial settings, such as factories, building sites, and shipping ports [1]. This is because they are good at lifting heavy loads across long distances. However, from a control engineering point of view, these systems are very challenging to work with, especially as the load moves like a pendulum. A trolley that moves along a fixed track and a load that hangs from a cable are common parts of an overhead crane. This means that the system's dynamics are nonlinear and connected. These adjustments make the load move in ways that aren't desirable, especially whether it speeds up or slows down. If this swing isn't handled effectively, it can make things less efficient and put people and adjacent equipment at risk [2]. Overhead cranes are typically classified as underactuated systems, as the number of independent actuators is insufficient to directly control all degrees of freedom of motion. Because it's hard to control all of the system's states at once, this lack of actuation makes it difficult to

control. No actuator can directly change the swing angle of the load. Instead, the trolley's movement must indirectly suppress it [3].

There has been a lot of research on how to make both simple and complicated control systems for overhead crane systems in the last several years. Park et al. developed a nonlinear feedback linearization controller for container cranes to make sure that the trolley is placed correctly and that the swing is stopped quickly, even with ropes of different lengths. This showed that the tracking was good and the transient performance could be changed [4]. Cao and Liu proposed an adaptive fuzzy sliding mode controller that utilizes Lyapunov-based adaptation to address variations in rope length and load mass, demonstrating effective performance in accommodating these changes [5]. Smoczek et al. employed a fuzzy logic controller integrated with pole positioning and a stereovision system to detect sway non-contractually. They effectively utilized it in production processes [6]. In [7], Midhat proposed a sliding mode controller (SMC) that was more stable, better at damping swings, and more durable than PID control. Khudhair et al. developed a Backstepping controller for overhead cranes and validated robustness under ±20% parameter uncertainties. The method reduced swing by over 50% and cut control energy consumption by up to 70%, perfecting Fuzzy Logic control [8]. Zehar et al. introduced Fast Terminal Synergetic Control (FTSC) to eliminate chattering while ensuring finite-time stability and enhanced precision [9]. Miao et al. integrated the Harmony Search (HS) algorithm with a Radial Basis Function (RBF) neural network to generate smooth trolley trajectories that accounted for wind and air resistance, resulting in significant swing reduction and improved operational efficiency [10]. Hussein et al. compared SMC and LQR and found that SMC worked better in both steady-state and transient scenarios when the parameters varied [11]. Lastly, Al-Saedi et al. presented a feedforward–feedback fuzzy logic controller that demonstrated enhanced robustness and disturbance rejection in 2D crane operations; nevertheless, the effects of variations in mass and rope length were not addressed [12]. This study's main contributions are explained as follows:

- Examine two controller methods: synergetic control (SC) and feedback linearization-based state feedback controller (FL-SFC) which are applied to the control the overhead crane system to a certain position with as little swing as possible.
- To enhance the two controllers (SC and FL-SFC), flower pollination algorithm (FPA) is introduced to find the optimal value of the design variables of each controller.
- Lyapunov function is employed to provide a mathematically rigorous way to prove system stability of the synergetic control

The next parts of the paper are set up like this: In Section 2, the mathematical model and equations of motion for the overhead crane system is given. Section 3 explains how to combine the control laws of FL-SFC and SC. Section 3.3 describes the flower pollination algorithm. Section 4 shows the findings of the simulation study. Section 5 contains the conclusion.

2. Mathematical Model

In this study, a simplified yet accurate anti-swing dynamic model of the bridge crane system is developed. Due to the inherent complexity of the crane, which is categorized as an underactuated mechanical system, the modeling approach aims to reduce system complexity without compromising essential dynamics. Therefore, two assumptions were made: the impact of wind and air resistance is considered negligible, and the study is limited to the two-dimensional plane of the trolley and its suspended load. To analyze the motion of the bridge crane system, a two-dimensional coordinate system is established, with the origin placed at point O (0, 0). The physical structure of the crane is illustrated schematically in Fig. 1 showing the system layout and the other representing its coordinates in the X–Y plane [13]. Within this framework:

- M refers to the mass of the crane trolley (kg),

- m denotes the mass of the suspended load (Kg),
- L is the length of the hoisting rope (m),
- X represents the horizontal position of the trolley (m),
- θ is the angular displacement (swing angle) of the load from the vertical (rad),
- F indicates the external force applied to move the trolley (N),
- g stands for gravitational acceleration (m/s²).

Under these assumptions, the dynamic behavior of the system is derived using the Lagrangian method. Lagrange's equation is a fundamental tool in classical mechanics used to derive the equations of motion for dynamic systems [14], [15]. It provides a structured way to model mechanical systems using energy principles and is written in the general form as:

$$\begin{gathered} L(q,\dot{q}) = T(q,\dot{q}) - V(q,\dot{q}) \\ \frac{d}{dt}\left(\frac{\partial L}{\partial \dot{q}_k}\right) - \frac{\partial L}{\partial q_k} - Q_k = 0 \end{gathered} \tag{1}$$

where k =1,2,n; L is the Lagrangian; T is the kinetic energy of the system; V is the potential energy of the system; $q_k$is a set of generalized coordinates; and $Q_k$is the generalized inertia force. Thus, the dynamic model of the bridge crane can be described as follows:

$$\begin{gathered} (M+m)\ddot{x} + m\ddot{l}\sin\theta + 2m\dot{l}\,\dot{\theta}\cos\theta - ml\dot{\theta}^2\sin\theta = F \\ 2\dot{l}\dot{\theta} + l\dot{\theta} + \ddot{x}\cos\theta + g\sin\theta = 0 \\ m\ddot{l} + m\ddot{x}\sin\theta - ml\dot{\theta}^2 - mg\cos\theta = F \end{gathered} \tag{2}$$

Assuming that the rope length satisfies $\dot{l} = \ddot{l} = 0$. Thus, the simplified crane model can be expressed as:

$$\begin{gathered} (M+m)\ddot{x} + ml\ddot{\theta}\cos\theta = F + ml\dot{\theta}^2\sin\theta \\ l\dot{\theta} + \ddot{x}\cos\theta - g\sin\theta = 0 \end{gathered} \tag{3}$$

Eq. (3) can be rearranged into a following differential equation about the angle θ and displacement *x*.

$$\begin{gathered} \ddot{\theta} = \frac{-F\cos\theta - l\dot{\theta}^2\cos\theta\sin\theta - mg\sin\theta - Mg\sin\theta}{(M + m\,x\,\sin^2\theta)l} \\ \ddot{x} = \frac{F + l\dot{\theta}^2\sin\theta + mg\sin\theta\cos\theta}{(M + m\,x\,\sin^2\theta)} \end{gathered} \tag{4}$$

Now, the following variables are defined: x_1= θ, x_2= $\dot{\theta}$, x_3= x, x_4=$\dot{x}$, the differential equation of the crane system can be stated as follows:

$$\begin{gathered} \dot{x_1} = \dot{\theta} = x_2 \\ \dot{x_2} = \ddot{\theta} = \frac{-F\cos\theta - l\dot{\theta}^2\cos\theta\sin\theta - mg\sin\theta - Mg\sin\theta}{(M + m\,x\,\sin^2\theta)l} \\ \dot{x_3} = x_4 \\ \dot{x_4} = \ddot{x} = \frac{F + l\dot{\theta}^2\sin\theta + mg\sin\theta\cos\theta}{(M + m\,x\,\sin^2\theta)} \end{gathered} \tag{5}$$

The crane system can be written in the following form:

$$\begin{aligned} \dot{x}_1 &= x_2 \\ \dot{x}_2 &= f_1(x) + g_1(x)\, u \\ \dot{x}_3 &= x_4 \\ \dot{x}_4 &= f_2(x) + g_2(x)\, u \end{aligned} \tag{6}$$

Where

$f_1(x) = \frac{-lx_2^2 \cos x_1 \sin x_1 - mg\sin x_1 - Mg\sin x_1}{(M+m\sin^2 x_1)l}$

$g_1(x) = \frac{-\cos x_1}{(M+m\sin^2 x_1)l}$

$f_2(x) = \frac{lx_2^2 \sin x_1 - mg\sin x_1 \cos x_1}{M+m\sin^2 x_1}$

$g_2(x) = \frac{1}{M+m\sin^2 x_1}$

In this case, u is the control input, and $f_1(x)$, $f_2(x)$, g_1, and g_2 are nonlinear functions.

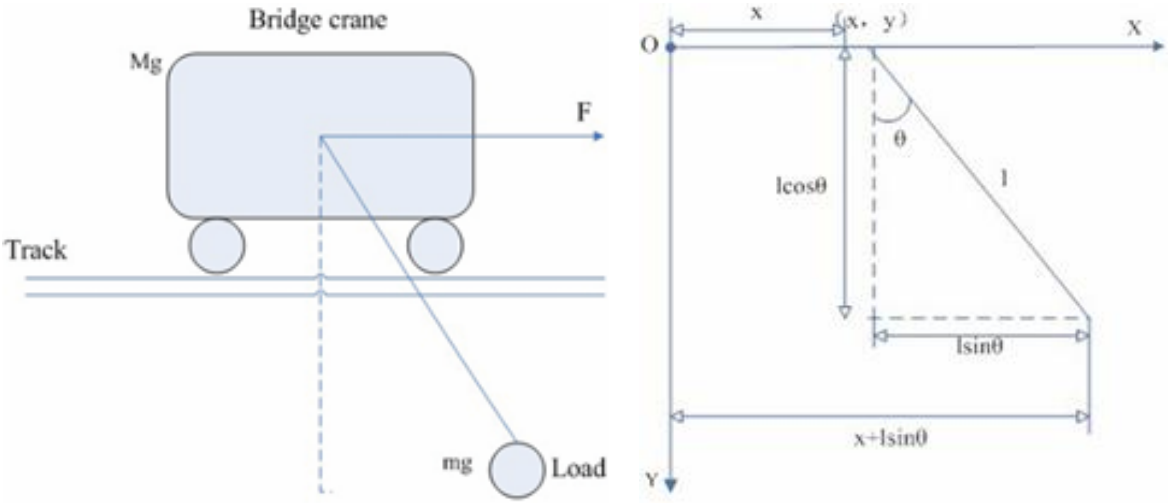

(a) (b)

Fig. 1. (a) The two-dimensional layout of the crane system. (b) X − Y plots of the crane system

3. Controller Design

Feedback controllers [16]-[22] are presently used to control a number of systems. Ensuring smooth operation of the overhead crane system requires addressing several inherent challenges and control-related issue. For instance, the system must accurately track the desired trajectory while suppressing load oscillations induced by external disturbance. In this work, two nonlinear control strategies were employed to find the control law for the overhead crane: Synergetic Control (SC) and Feedback Linearization with State Feedback Control (FL-SFC).

3.1. Synergetic Control

SC is a well-established nonlinear control method that has changed a lot of control design applications. Synergetic control utilizes the concept of a model of the system to formulate the control law [23]. Let's define e_θ as the error between the actual and the desired angular position outputs:

$$e_\theta = \theta_r - x_3 \tag{7}$$

Taking the first and the second derivative of the error gives:

$$\dot{e}_\theta = \dot{\theta}_r - \dot{x}_3 \tag{8}$$

$$\ddot{e}_\theta = \ddot{\theta}_r - \dot{x}_4 \tag{9}$$

Define a macro-variable ψ_θ, the macro-variable ψ is selected as:

$$\psi_\theta = c_1 e_\theta + \dot{e}_\theta \tag{10}$$

Taking the derivative of the macro-variable ψ gives:

$$\dot{\psi}_\theta = c_1 \dot{e}_\theta + \ddot{e}_\theta \tag{11}$$

Where c_1 (c_1>0) is a scalar designing parameter

To assure stability (i.e. to make sure that the state trajectories travel toward the intended manifolds and stay there), let's define the following:

$$\dot{\psi}_\theta + T_1 \psi_\theta = 0 \tag{12}$$

$$\dot{\psi}_\theta = -T_1 \psi_\theta \tag{13}$$

Where $T_1 (T_1 > 0)$ is an adjustable parameter that signifies the rate of convergence to the intended manifolds.

Substituting Eq. (11) in Eq. (12) gives:

$$c_1 \dot{e}_\theta + \ddot{e}_\theta + T_1 \psi_\theta = 0 \tag{14}$$

By substituting Eq. (9) in Eq. (14), we obtain:

$$c_1 \dot{e}_\theta + \ddot{\theta}_r - \dot{x}_4 + T_1 \psi_\theta = 0 \tag{15}$$

Using the 4th equation in Eq. (6) obtains:

$$c_1 \dot{e}_\theta + \ddot{\theta}_r - f_1(x) - g_1(x) u_1 + T_1 \psi_\theta = 0 \tag{16}$$

Select u_1 as follows:

$$u_1 = \frac{1}{g_1(x)} (c_1 \dot{e}_\theta + \ddot{\theta}_r - f_1(x) + T_1 \psi_\theta) \tag{17}$$

Let's define e_x as the error between the actual and the desired linear position outputs:

$$e_x = x_r - x_1 \tag{18}$$

Taking the first and the second derivative of the error gives:

$$\dot{e}_x = \dot{x}_r - \dot{x}_1 \tag{19}$$

$$\ddot{e}_x = \ddot{x}_r - \dot{x}_2 \tag{20}$$

Define a macro-variable ψ_x, the macro-variable ψ_x is selected as:

$$\psi_x = c_2 e_x + \dot{e}_x \tag{21}$$

Taking the derivative of the macro-variable ψ_x gives:

$$\dot{\psi}_x = c_2 \dot{e}_x + \ddot{e}_x \tag{22}$$

Where c_2 (c_2>0) is a scalar designing parameter

The desired dynamic evolution of the macro-variable is:

$$\dot{\psi}_x + T_2\psi_x = 0 \tag{23}$$

$$\dot{\psi}_x = -T_2\psi_x \tag{24}$$

Where $T_2(T_2 > 0)$ is an adjustable parameter that signifies the rate of convergence to the intended manifolds.

Substituting Eq. (22) in Eq. (23) gives:

$$c_2\dot{e}_x + \ddot{e}_x + T_2\,\psi_x = 0 \tag{25}$$

By substituting Eq. (20) in Eq. (25), we obtain:

$$c_2\dot{e}_x + \ddot{x}_r - \dot{x}_2 + T_2\,\psi_x = 0 \tag{26}$$

This yield:

$$c_2\dot{e}_x + \ddot{x}_r - f_2(x) - g_2(x)\,u_2 + T_2\,\psi_x = 0 \tag{27}$$

Select u_2 as follows:

$$u_2 = \frac{1}{g_2(x)}\,(c_2\dot{e}_x + \ddot{x}_r - f_2(x) + T_2\,\psi_x) \tag{28}$$

Choose the Lyapunov function as:

$$V = \frac{1}{2}\psi_\theta^2 + \frac{1}{2}\psi_x^2 \tag{29}$$

Taking the derivative of V gives:

$$\dot{V} = \psi_\theta\dot{\psi}_\theta + \psi_x\dot{\psi}_x \tag{30}$$

Substitute Eq. (13) and Eq. (24) in Eq. (30):

$$\dot{V} = \psi_\theta(-T_1\,\psi_\theta) + \psi_x(-T_2\,\psi_x) \tag{31}$$

$$\dot{V} = -T_1\psi_\theta^2 - T_2\psi_x^2 \tag{32}$$

We get $\dot{V} < 0$, which means that the system is stable.

Thus, the final control law of SC is given by:

$$U = u_1 + u_2 \tag{33}$$

3.2. Feedback Linearization-Based State Feedback Controller

The feedback linearization (FL) technique is a well-established method for trajectory tracking in nonlinear systems [24]-[27]. This method formulates the control law to transform the original nonlinear system into an equivalent linear representation, as articulated:

$$U_1 = \frac{1}{g_1(x)}(-f_1(x) + u_{l1}) \tag{34}$$

$$U_2 = \frac{1}{g_2(x)}(-f_2(x) + u_{l2}) \tag{35}$$

$$U = U_1 + U_2 \tag{36}$$

Where u_{l1}, u_{l2} can be any linear controller. In this paper, a state feedback controller (SFC) is selected as follows:

$$ul_1 = -k_1x_1 - k_2x_2 \tag{37}$$

$$ul_2 = k_3(x_r - x_3) - k_4x_4 \tag{38}$$

where $k_1, k_2, k_3,$ and k_4 are the SFC gains that are set up to get the desired tracking performance.

3.3. Flower Pollination Algorithm

Swarm optimization techniques have become gradually popular to obtain global solution for a wide-range of engineering problems [28]-[33]. Within the field of control engineering, adjusting controllers remains a longstanding and essential element of feedback control. Several authors and scholars presented different swarm optimization techniques to tune the design parameters of the feedback controller [34]-[41]. In this paper, flower pollination algorithm is proposed to tune the design parameters of the SC and FL-SFC. Flower pollination usually means moving pollen, which is often done by creatures like insects, birds, bats, and other animals. Certain flowers and insects have indeed evolved together to form a very specific interaction between flowers and pollinators. Some flowers only attract and depend on certain types of insects for pollination to work. There are two main types of pollination: abiotic and biotic. About 90% of blooming plants use biotic pollination, which means that pollinators like insects and mammals spread pollen. About 10% of pollination happens without the help of pollinators, which is called abiotic pollination. Wind and diffusion in water help flowering plants get pollen [42]. Pollinators are known as pollen carriers. This method has two fundamental steps: global pollination and local pollination. The Pseudo code of the Flower Pollination Algorithm is given in Algorithm 1.

Algorithm1. Pseudo code of the Flower Pollination Algorithm

1- Objective min or max f(x), Fx = (Fx1,Fx2,...,Fxd)
2- Initialize a population of n flowers/pollen gametes with random solutions
3- Find the best solution x_g in the initial population.
4- Define a switch probability p ∈ [0,1].
5- **while** (t < Max Generation)
6- **for** i = 1 : n (all n flowers in the population)
7- **if** rand < p,
8- Draw a (d-dimensional) step vector ρ which obeys a L´evy distribution
9- Global pollination via $Fx_i^{t+1} = Fx_i^t + \rho(x_g - x_i^t)$
Else
10- Draw ϵ from a uniform distribution in [0,1] .
11- Randomly choose j and k among all the solutions.
12-Do local pollination via $Fx_i^{t+1} = Fx_i^t + \epsilon(x_j^t - x_k^t)$
end if
13- Evaluate new solutions
14-If new solutions are better, update them in the population.
end for
15- Find the current best solution x_g
end while

In the global pollination process, floral pollen is transported by pollinators, such as insects, which are capable of traversing considerable distances due to their ability to fly and navigate extensive ranges. This guarantees the pollination and reproduction of the fittest individuals,

represented as x_g. The initial rule, together with floral constancy, can be mathematically expressed as.

$$Fx_i^{t+1} = Fx_i^t + \rho(x_g - Fx_i^t) \quad (39)$$

Where Fx_i^t is the pollen i or solution vector Fx_i at iteration t, and x_g represents the optimal solution identified among all solutions in the current generation/iteration. The parameter ρ represents the intensity of pollination, effectively functioning as a step size [43]. Insects can traverse considerable distances using varied step lengths; thus, we can effectively employ a Lévy flight to simulate this behavior. We sample ρ > 0 from a Lévy distribution.

$$\rho \sim \frac{\lambda\Gamma(\lambda)\sin(\pi\lambda/2)}{\pi}\frac{1}{s^{1+\lambda}} \ (s \gg s0 > 0) \quad (40)$$

In this context, Γ(λ) is the standard gamma function, and this distribution is applicable for substantial steps s > 0. All simulations presented below utilize λ = 1.5. Local pollination and floral constancy can be expressed as [44]:

$$Fx_i^{t+1} = Fx_i^t + \epsilon(x_j^t - x_k^t) \quad (41)$$

Where x_j^t and x_k^t represent pollen from distinct flowers of the same plant species. This effectively replicates flower consistency within restricted vicinity. If $x_j^t$and x_k^t originate from the same species or are selected from the same population, this constitutes a local random walk when ϵ is drawn from a uniform distribution in the interval [0, 1]. Flower pollination activities can transpire on both local and global scales. In practice, nearby flower patches or blooms in close proximity are more likely to be pollinated by local pollen than those situated at a greater distance. To do this, we employ a switch probability or proximity probability p to transition from prevalent global pollination to concentrated values local pollination. Initially, we can utilize p = 0.5 and thereafter do a parametric research to determine the optimal parameter range [45].

4. Simulation Results

The simulation studies carried out to confirm the efficacy of the recommended control strategy are presented in this section. After that, the results are examined in order to evaluate performance in comparison.

4.1. Simulation Setup

MATLAB was used to simulate the overhead crane system under SC and FL-SFC control strategies. Table 1 provides a summary of the system parameters [13]. Fig. 2 and Fig. 3 show the structures of the SC and FL-SFC controllers that were optimized for the crane system using FPA. The reference position was set at 1 m, and the crane's initial trolley position and swing angle were set at 0 m and 0 rad, respectively.

Table 1. Crane parameters

Parameters	Values
The length of rope L	3m
Mass of the trolley M	2000kg
Mass of the load m	1000kg
Gravitational acceleration g	9.8m/s^2

Both controllers' design parameters are modified using the FPA algorithm to attain the best performance. By adjusting their respective parameters, namely (c_1, c_2, T_1, T_2) and (k_1, k_2, k_3, k_4), the SC and FL-SFC controllers' efficacy is increased. The Integral of Absolute Errors (IAE) is the

cost function used to check and change how well the two controllers work, as shown in Eq. (42) [46]-[50].

$$\begin{aligned} IAE_{\theta} &= \int_{0}^{t=tsim} |e_{\theta}(t)|dt \\ IAE_{x} &= \int_{0}^{t=tsim} |e_{x}(t)|dt \\ IAE_{T} &= IAE_{\theta} + IAE_{x} \end{aligned} \tag{42}$$

Where $tsim$ represents the total simulation time, Table 2 shows the values parameters that were chosen for the design controllers.

Table 2. Optimal setting of the controllers

Controller	Parameters	Values
SC	c_1	5
	c_2	350
	T_1	290
	T_2	0.3
FL-SFC	k_1	966
	k_2	88
	k_3	66
	k_4	180

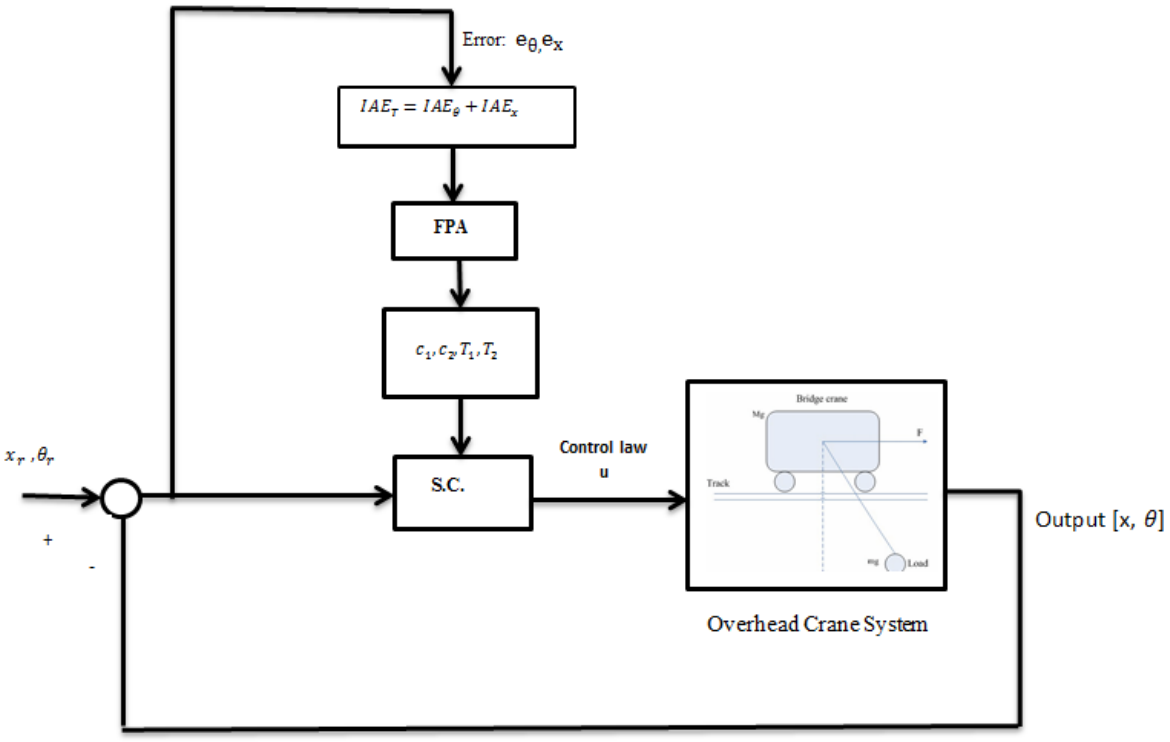

Fig. 2. Proposed SC controller tuned by FPA

4.2. Evaluation in Normal Conditions

Fig. 4 shows how the crane system reacted to the step input. Comparing the two control methods (SC and FL-SFC), the IAEx for tracking the trolley's location is 342.7605 for SC and 349.3791 for FL-SFC also the SC has 1.1 5 overshoot and the settling time (ts) is reduced to 7.4 s in contrast to the FL-SFC, where the overshoot reaches 8.5% and settling time (ts) is 12.5 s, Fig. 5 illustrates that the IAEθ for swing angle suppression is 4.8422 with the SC controller and 5.5070

with the FL-SFC controller, For the SC, the obtained Δθ (0.021) was significantly smaller, indicating superior swing suppression and enhanced damping performance, on the other hand, the SFC exhibited a larger Δθ (0.024), demonstrating higher oscillatory behavior and less effective suppression of the load swing. This comparison shows that both controllers can manage the crane system with zero steady-state error ($es.s$) and confirms that the SC achieves better stabilization of the swing angle by minimizing the oscillatory range, whereas the SFC results in greater angular fluctuations before settling. Transient performance of the crane system (nominal condition) shown in Table 3.

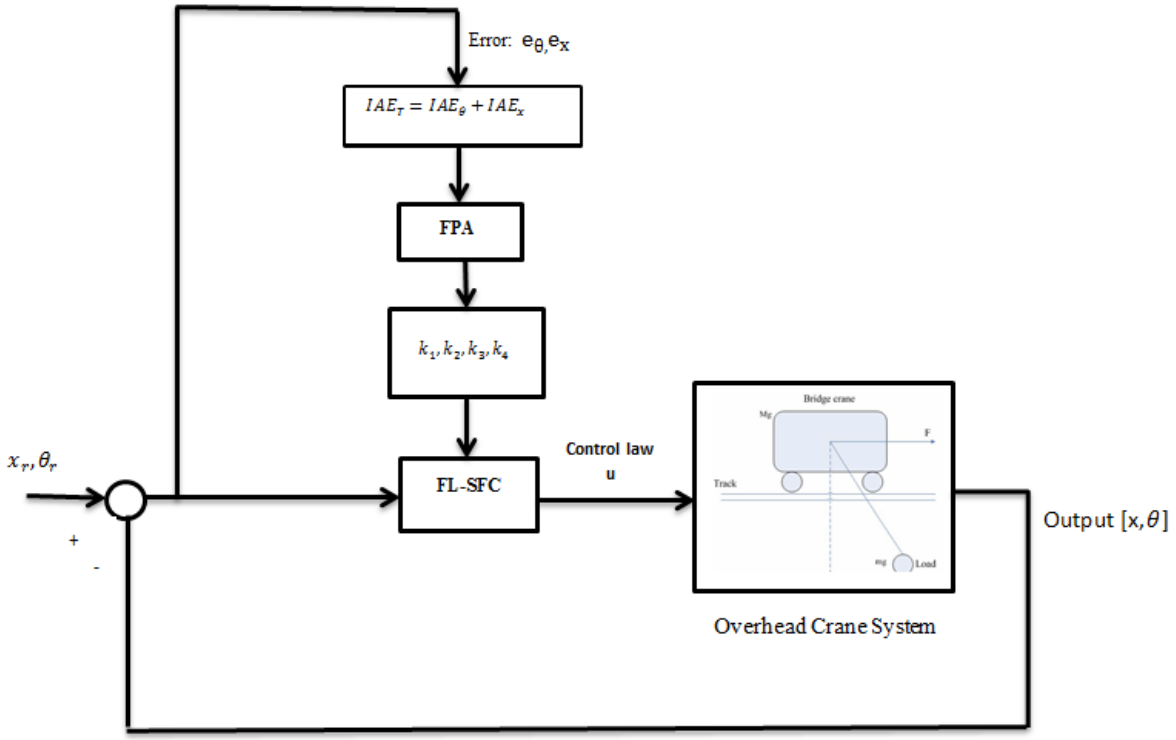

Fig. 3. Proposed FL-SFC controller tuned by FPA

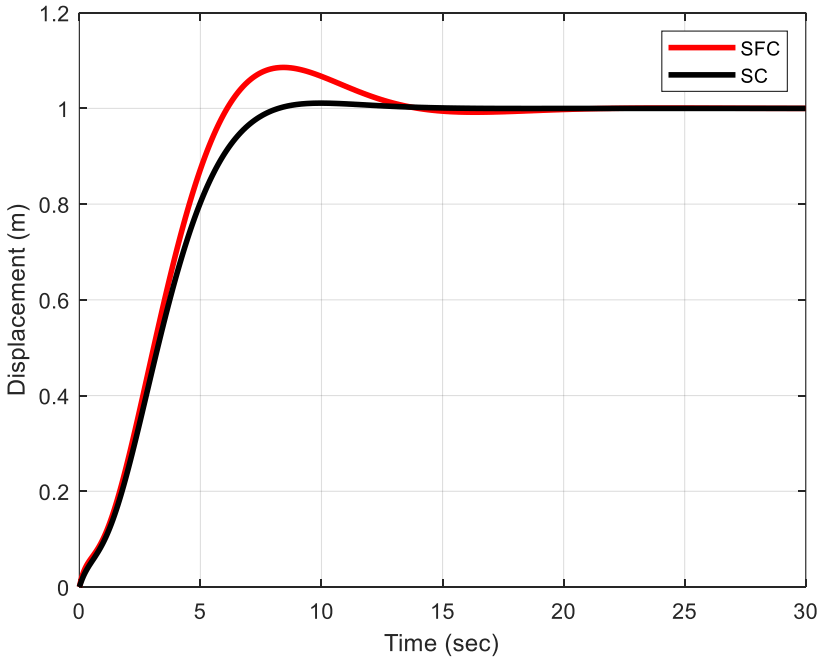

Fig. 4. Position's response of crane system

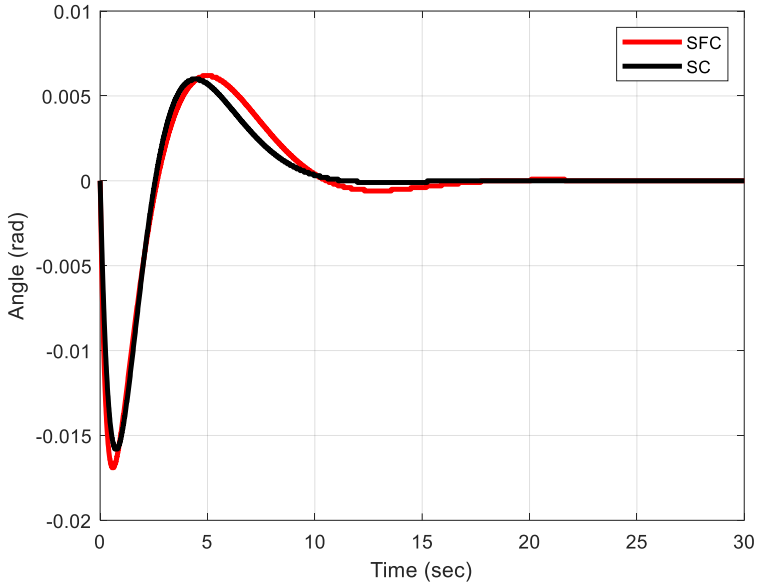

Fig. 5. Angle's response of crane system

Table 3. Transient performance of the crane system (nominal condition)

Controller	IAE_x	IAE_θ	Overshoot	Settling time 2%	Δθ
SC	342.76	4.842	1.1%	7.4 s	0.021 rad
FL-SFC	349.38	5.507	8.5%	12.5 s	0.024 rad

4.3. Evaluation Under Mass Uncertainty

In practical applications, the overhead crane's payload mass is not constant and may vary according to the type of material being lifted or transported. Therefore, to evaluate the robustness of the proposed controllers under load mass uncertainty, the payload mass is assumed to fluctuate by ±20% of its nominal value. Fig. 6 and Fig. 7 illustrate the response of the two controlled systems when the payload mass of the system is increased by 20%. The corresponding numerical value of the time response is reported in Table 4. Moreover, Fig. 8 and Fig. 9 show the response of the two controlled systems when the payload mass of the system is decreased by 20%. The corresponding numerical value of the time response is reported in Table 5.

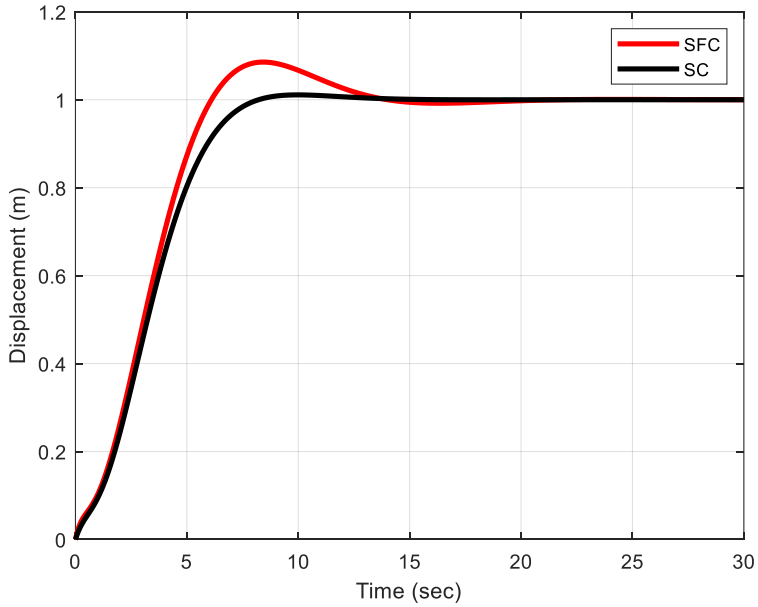

Fig. 6. Position's response when the payload mass of crane system increased 20%

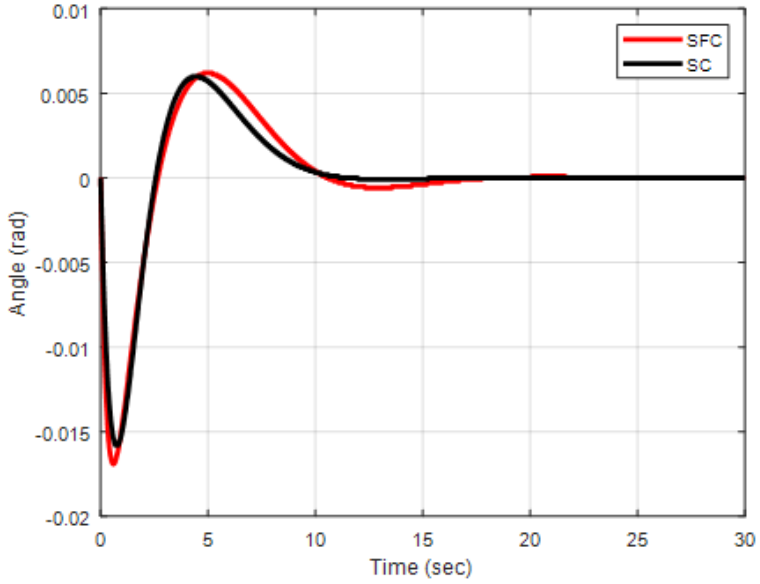

Fig. 7. Angle's response when the payload mass of crane system increased 20%

Table 4. Transient performance when the payload mass of crane system increased 20%

Controller	IAE_x	IAE_θ	Overshoot	Settling time 2%	Δθ
SC	342.785	4.842	1.1%	7.4 s	0.0218 rad
FL-SFC	349.446	5.507	10%	12.4 s	0.023 rad

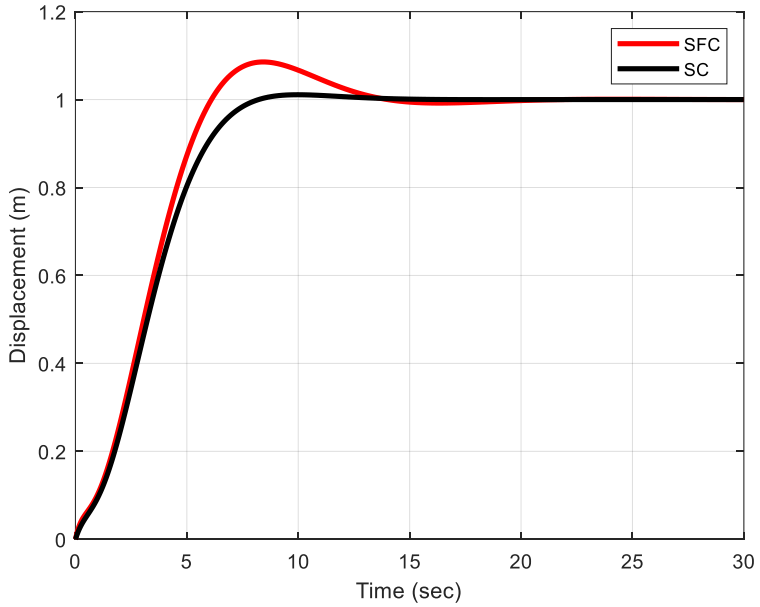

Fig. 8. Position's response when the payload mass of crane system decreased 20%

Table 5. Transient performance when the payload mass of crane system decreased 20%

Controller	IAE_x	IAE_θ	Overshoot	Settling time 2%	Δθ
SC	342.73	4.84	1.1%	7.4 s	0.021 rad
FL-SFC	349.31	5.50	10%	12.4 s	0.022 rad

The results indicate that the SC has stronger robustness for controlling the overhead crane system under ±20% load-mass uncertainty, achieving superior trolley-position tracking x and more

effective sway suppression θ. Consequently, the SC controller improves positioning precision and operational smoothness in the presence of payload-mass fluctuations.

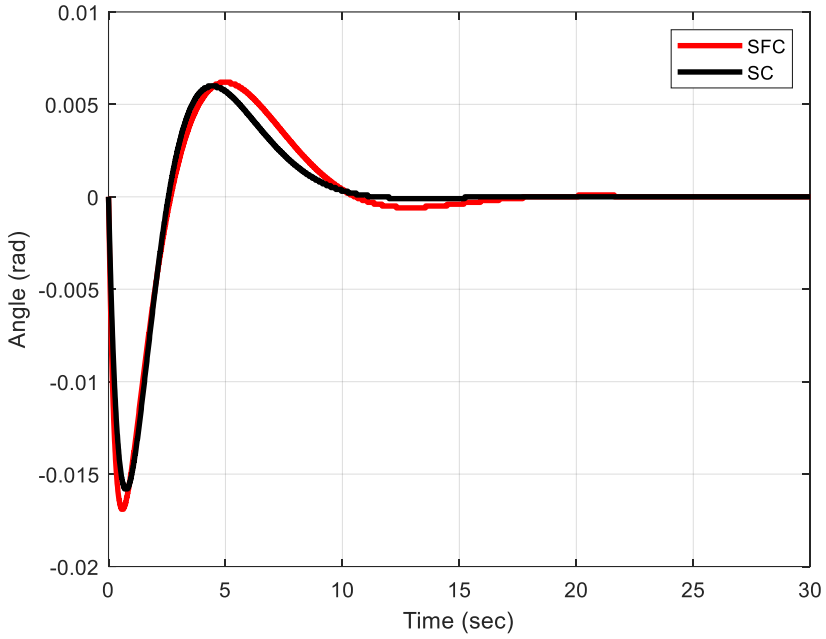

Fig. 9. Angle's response when the payload mass of crane system decreased 20%

4.4. Evaluation Under Rope Length Uncertainty

In practical cranes, rope length of the crane system is not fixed. Evaluating the performance of the controller at multiple lengths ensures it works under real-world scenarios. Therefore, to evaluate the robustness of the proposed controllers under rope length uncertainty, the rope length is assumed to fluctuate by ±20% of its nominal value. Fig. 10 and Fig. 11 illustrate the response of the two controlled systems when the rope length of the system is increased by 20%. The corresponding numerical value of the time response is reported in Table 5. Moreover, Fig. 12 and Fig. 13 show the response of the two controlled systems when the rope length of the system is decreased by 20%. The corresponding numerical value of the time response is reported in Table 6.

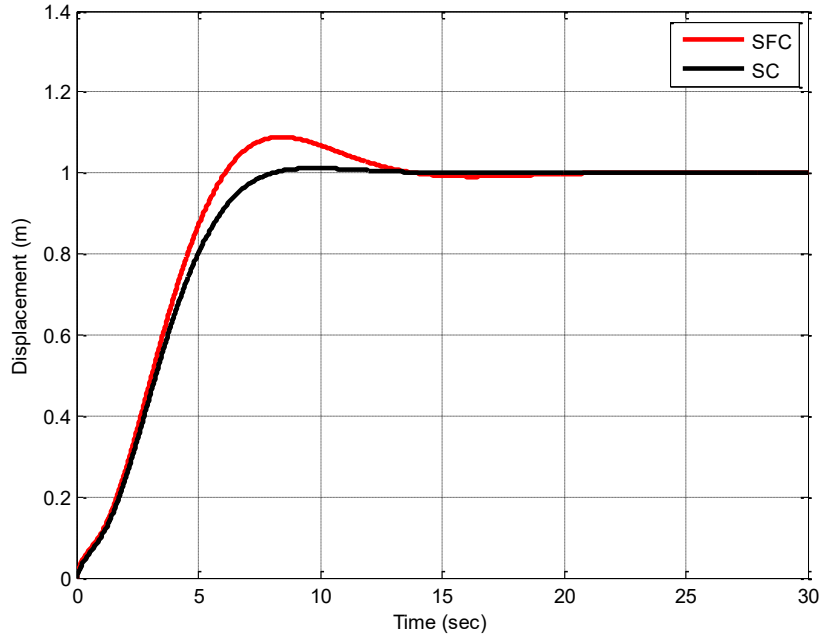

Fig. 10. Position's response when the rope length of crane system increased 20%

The results indicate that the SC has stronger robustness for controlling the overhead crane system under ±20% rope length uncertainty, achieving superior trolley-position tracking x and more effective sway suppression θ. Consequently, the SC controller improves positioning precision and operational smoothness in the presence of payload-mass fluctuations. Transient performance when the rope length of crane system decreased 20% shown in Table 7.

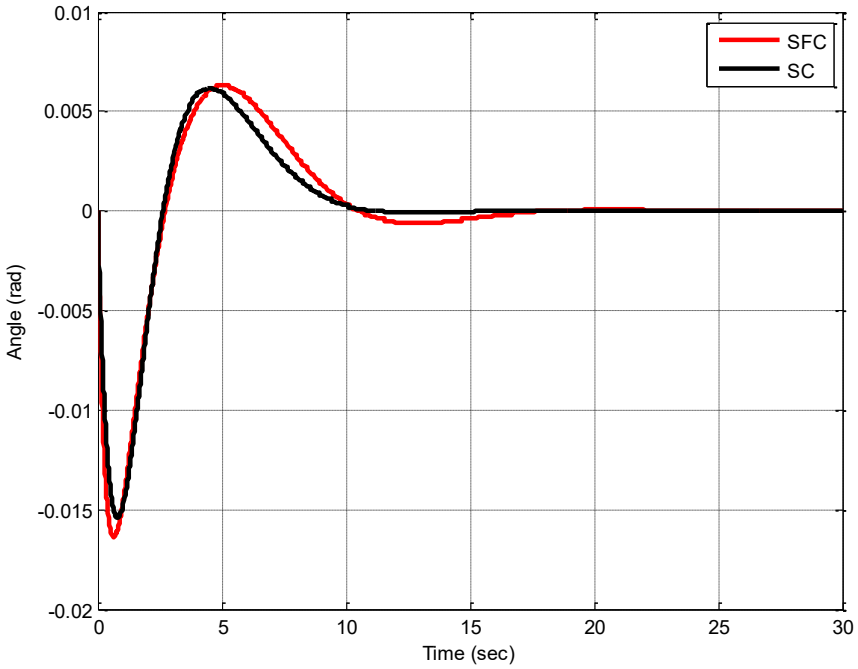

Fig. 11. Angle's response when the rope length of crane system increased 20%

Table 6. Transient performance when the rope length of crane system increased 20%

Controller	IAE_x	IAE_θ	Overshoot	Settling time 2%	Δθ
SC	343.05	4.89	1.1%	7.3 s	0.021 rad
FL-SFC	351.53	5.58	8.8%	12.3 s	0.022 rad

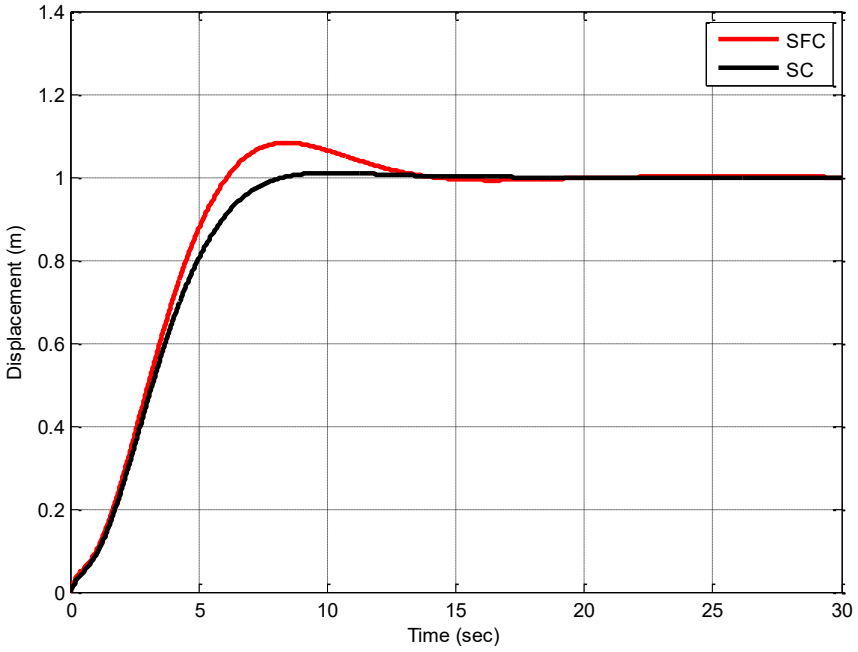

Fig. 12. Position's response when the rope length of crane system decreased 20%

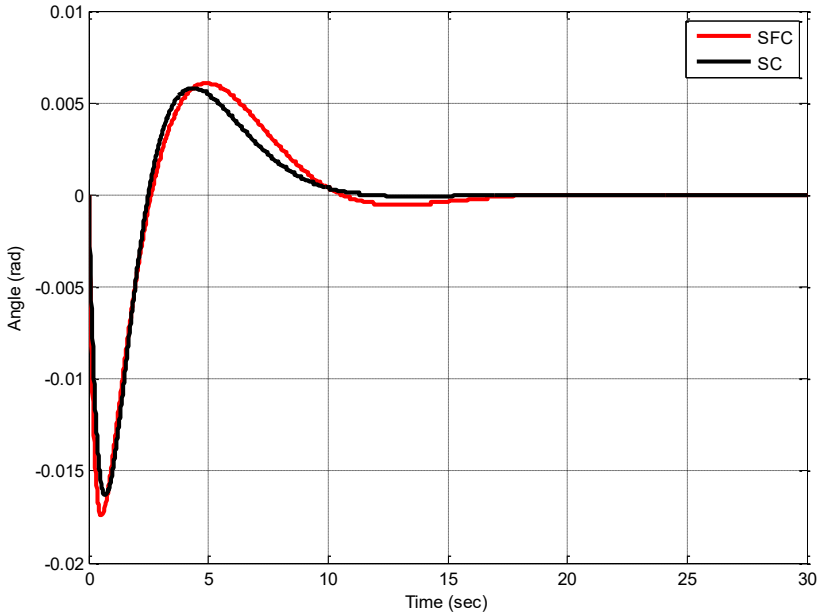

Fig. 13. Angle's response when the rope length of crane system decreased 20%

Table 7. Transient performance when the rope length of crane system decreased 20%

Controller	IAE_x	IAE_θ	Overshoot	Settling time 2%	Δθ
SC	342.5	4.8	1%	7.5 s	0.022 rad
FL-SFC	347.4	5.5	8.2%	12.5 s	0.023 rad

5. Conclusion

This paper presented a comparative control study for a 2-D overhead-crane system using Synergetic Control (SC) and Feedback-Linearization-based State-Feedback (FL-SFC) designs. Both controllers were tuned via the Flower Pollination Algorithm (FPA) under a unified performance criterion, and evaluated on trolley-position tracking and sway suppression. From a control perspective, the results demonstrate that SC yields more favorable transient and integral-error characteristics than FL-SFC under nominal conditions. Specifically, FL-SFC exhibits a percent overshoot of = 8.5% in the trolley position with a settling time of = 12.5 s, whereas SC shows 1.1 % overshoot and a shorter settling time, reflecting faster yet well-damped convergence. Integral-error indices further corroborate this trend: IAEx=342.7605 for SC vs. IAEx=349.3791 for FL-SFC, and IAEθ=4.8422 for SC vs. IAEθ 5.5070 for FL-SFC, indicating improved tracking and sway attenuation with SC. Qualitatively, SC also achieves smaller sway amplitudes (lower $\Delta\theta$) and quicker damping of $\theta(t)$, consistent with the macro-variable/invariant-manifold design that shapes the closed-loop transient. Robustness assessments under ±20% payload-mass and rope length uncertainties show that SC maintains superior transient behavior and reduced sensitivity to parametric variations relative to FL-SFC. This aligns with the known sensitivity of feedback-linearization to model mismatch. Taken together, the evidence supports adopting SC as a strong baseline controller for overhead-crane anti-sway and positioning tasks, while FL-SFC remains competitive when model accuracy is high and operating points are well characterized. Future work may consider extending the framework toward observer-based implementations (to relax full-state measurement), adaptive/scheduled variants to handle wider mass/rope-length ranges, and additional robustness tests (e.g., wind disturbances, actuator limits and anti-windup) to further characterize closed-loop performance in operational settings.

Author Contribution: All authors contributed equally to the main contributor to this paper. All authors read and approved the final paper.

Funding: This research received no external funding.

Conflicts of Interest: The authors declare no conflict of interest.

References

[1] M. S. Mahmoud, N. M. Alyazidi, and A. M. Hassanine, "Modeling and control of underactuated three-dimensional overhead crane systems," *International Journal of Robotics and Automation Technology*, vol. 6, pp. 80-85, 2019, https://doi.org/10.31875/2409-9694.2019.06.10.

[2] N. T. Vu, "LMI based antiswing adaptive controller for uncertain overhead cranes," *International Journal of Electrical & Computer Engineering*, vol. 10, no. 6, pp. 5793-5801, 2020, http://doi.org/10.11591/ijece.v10i6.pp5793-5801.

[3] B. Rong, X. Rui, L. Tao, and G. Wang, "Dynamics analysis and fuzzy anti-swing control design of overhead crane system based on Riccati discrete time transfer matrix method," *Multibody System Dynamics*, vol. 43, no. 3, pp. 279-295, 2018, https://doi.org/10.1007/s11044-017-9598-z.

[4] H. Park, D. Chwa, and K. Hong, "A feedback linearization control of container cranes: Varying rope length," *International Journal of Control Automation and Systems*, vol. 5. no. 4, pp. 379-387, 2007, https://www.koreascience.kr/article/JAKO200734514836371.page?&lang=en.

[5] L. Cao and L. Liu, "Adaptive Fuzzy Sliding Mode Method-Based Position and Anti-swing Control for Overhead Cranes," *2011 Third International Conference on Measuring Technology and Mechatronics Automation*, pp. 335-338, 2011, https://doi.org/10.1109/ICMTMA.2011.85.

[6] J. Smoczek, J. Szpytko, and P. Hyla, "The application of an intelligent crane control system," *IFAC Proceedings Volumes*, vol. 45, no. 24, pp. 280-285, 2012, https://doi.org/10.3182/20120912-3-BG-2031.00058.

[7] F. Zhang, J. Geng, Z. Chen, L. Zhou, X. Shao and J. Zhang, "Fractional-Order Sliding Mode Control for a Container Crane System," *2024 14th Asian Control Conference (ASCC)*, pp. 1-6, 2024, https://ieeexplore.ieee.org/abstract/document/10665446.

[8] M. Y. Khudhair, M. Y. Hassan, and S. K. Kadhim, "Backstepping control strategy for overhead crane system," *Engineering and Technology Journal*, vol. 39, no. 3A, pp. 370-381, 2021, https://doi.org/10.30684/etj.v39i3A.1738.

[9] R. T. Cahyono, S. P. Kenaka and B. Jayawardhana, "Simultaneous Allocation and Scheduling of Quay Cranes, Yard Cranes, and Trucks in Dynamical Integrated Container Terminal Operations," *IEEE Transactions on Intelligent Transportation Systems*, vol. 23, no. 7, pp. 8564-8578, 2022, https://doi.org/10.1109/TITS.2021.3083598.

[10] Y. Miao, F. Xu, Y. Hu, J. An, and M. Zhang, "Anti-swing control of the overhead crane system based on the harmony search radial basis function neural network algorithm," *Advances in Mechanical Engineering*, vol. 11, no. 3, pp. 1-10, 2019, https://doi.org/10.1177/1687814019834458.

[11] E. Q. Hussein, A. Q. Al-Dujaili, and A. R. Ajel, "Design of sliding mode control for overhead crane systems," *IOP Conference Series: Materials Science and Engineering*, vol. 881, no. 1, p. 012084, 2020, https://doi.org/10.1088/1757-899X/881/1/012084.

[12] M. I. Al-Saedi, "Enhancing the feedforward–feedback controller for nonlinear overhead crane using fuzzy logic controller," *IOP Conference Series: Materials Science and Engineering*, vol. 745, no. 1, p. 012074, 2020, https://doi.org/10.1088/1757-899X/745/1/012074.

[13] Y. Li, S. Zhou and H. Zhu, "A backstepping controller design for underactuated crane system," *2018 Chinese Control And Decision Conference (CCDC)*, pp. 2895-2899, 2018, https://doi.org/10.1109/CCDC.2018.8407619.

[14] R. A. Kadhim, M. Q. Kadhim, H. Al-Khazraji, and A. J. Humaidi, "Bee algorithm based control design for two-links robot arm systems," *IIUM Engineering Journal*, vol. 25, no. 2, pp. 367-380, 2024, https://doi.org/10.31436/iiumej.v25i2.3188.

[15] K. Al-Badri, H. Dulaimi, H. Al-Khazraji, and A. J. Humaidi, "Adaptive Neural Network Control for Load-Varying Two-Link Robots Using Honey Badger Optimization," *Journal of Robotics and Control (JRC)*, vol. 6, no. 2, pp. 1061-1068, 2025, https://doi.org/10.18196/jrc.v6i2.26370.

[16] M. A. Al-Ali, O. F. Lutfy, and H. Al-Khazraj, "Investigation of optimal controllers on dynamics performance of nonlinear active suspension systems with actuator saturation," *Journal of Robotics and Control (JRC)*, vol. 5, no. 4, pp. 1041-1049, 2024, https://doi.org/10.18196/jrc.v5i4.22139.

[17] A. K. Ahmed and H. Al-Khazraji, "Optimal control design for propeller pendulum systems using gorilla troops optimization," *Journal Européen des Systèmes Automatisés*, vol. 56, no. 4, pp. 575-582, 2023, https://doi.org/10.18280/jesa.560407.

[18] N. X. Chiem, "Cascade control for trajectory-tracking mobile robots based on synergetic control theory and Lyapunov functions," *Control Systems and Optimization Letters*, vol. 3, no. 1, pp. 14-19, 2025, https://doi.org/10.59247/csol.v3i1.169.

[19] N. Setiawan, W. Caesarendra, and R. Majdoubi, "Implementation of Kalman Filter on Pid Control System for DC Motor Under Noisy Condition," *Buletin Ilmiah Sarjana Teknik Elektro*, vol. 6, no. 3, pp. 271-280, 2024, https://doi.org/10.12928/biste.v6i3.11236.

[20] A. K. Saber, S. A. Maged, M. Abdelaziz, and M. S. Mohamed, "Robust Velocity Control for a Launch Vehicle Erection System," *Journal of Robotics and Control (JRC)*, vol. 6, no. 4, pp. 1693-1709, 2025, https://doi.org/10.18196/jrc.v6i4.26385.

[21] F. R. T. Hasan, and S. A. Akbar, "PID Control Tuning Based on Wind Speed Sensor in Flying Robot," *Control Systems and Optimization Letters*, vol. 1, no. 3, 151-156, 2023, https://doi.org/10.59247/csol.v1i3.56.

[22] R. Al-Majeez, K. Al-Badri, H. Al-Khazraji and S.M. Ra'afat, "Design of A Backstepping Control and Synergetic Control for An Interconnected Twin-Tanks System: A Comparative Study," *International Journal of Robotics and Control Systems*, vol. 4, no. 4, pp. 2041-2054, 2024, https://doi.org/10.31763/ijrcs.v4i4.1682.

[23] H. Al-Khazraji, K. Al-Badri, R. Al-Majeez, and A. J. Humaidi, "Synergetic control design based sparrow search optimization for tracking control of driven-pendulum system," *Journal of Robotics and Control (JRC)*, vol. 5, no. 5, pp. 1549-1556, 2024, https://doi.org/10.18196/jrc.v5i5.22893.

[24] M. S. Xavier, A. J. Fleming and Y. K. Yong, "Nonlinear Estimation and Control of Bending Soft Pneumatic Actuators Using Feedback Linearization and UKF," *IEEE/ASME Transactions on Mechatronics*, vol. 27, no. 4, pp. 1919-1927, 2022, https://doi.org/10.1109/TMECH.2022.3155790.

[25] M. Vesović, R. Jovanović, and N. Trišović, "Control of a DC motor using feedback linearization and gray wolf optimization algorithm," *Advances in Mechanical Engineering*, vol. 14, no. 3, pp. 1-16, 2022, https://doi.org/10.1177/16878132221085324.

[26] F. R. Al-Ani, O. F. Lutfy, and H. Al-Khazraji, "Optimal Backstepping and Feedback Linearization Controllers Design for Tracking Control of Magnetic Levitation System: A Comparative Study," *Journal of Robotics and Control (JRC)*, vol. 5, no. 6, pp. 1888-1896, 2024, https://doi.org/10.18196/jrc.v6i1.24452.

[27] A. Hache, M. Thieffry, M. Yagoubi and P. Chevrel, "Control-Oriented Neural State-Space Models for State-Feedback Linearization and Pole Placement," *2022 10th International Conference on Systems and Control (ICSC)*, pp. 429-434, 2022, https://doi.org/10.1109/ICSC57768.2022.9993820.

[28] W. Aribowo and H. A. Shehadeh, "A Comparative Study of Metaheuristic Optimization Algorithms in Solving Engineering Designing Problems," *Journal of Robotics and Control (JRC)*, vol. 6, no. 4, pp. 1885-1898, 2025, https://doi.org/10.18196/jrc.v6i4.26410.

[29] R. Layona, B. Yulianto and Y. Tunardi, "Expedition Management Systems and Package Placement Optimization," *2025 5th International Conference on Innovative Research in Applied Science, Engineering and Technology (IRASET)*, pp. 1-6, 2025, https://doi.org/10.1109/IRASET64571.2025.11008314.

[30] A. Dafid *et al*., "Optimizing K-Nearest Neighbors with Particle Swarm Optimization for Improved Classification Accuracy," *Jurnal Ilmiah Teknik Elektro Komputer dan Informatika (JITEKI)*, vol. 11, no. 2, pp. 238-250, 2025, https://doi.org/10.26555/jiteki.v11i2.30775.

[31] H. Al-Khazraji, C. Cole and W. Guo, "Multi-objective particle swarm optimisation approach for production-inventory control systems," *Journal of Modelling in Management*, vol. 13, no. 4, pp.1037-1056, 2018, https://doi.org/10.1108/JM2-02-2018-0027.

[32] S. Tahcfulloh, D. Maulianawati, and D. Wiharyanto, "Optimizing 2.4GHz Wireless Networks in Shrimp Ponds with Particle Swarm Optimization," *Jurnal Ilmiah Teknik Elektro Komputer dan Informatika*, vol. 10, no. 4, pp. 817-832, 2024, https://doi.org/10.26555/jiteki.v10i4.30236.

[33] E. I. Muryadi, I. Futri, and D. C. E. Saputra, "iGWO-RF: an Improved Grey Wolfed Optimization for Random Forest Hyperparameter Optimization to Identification Breast Cancer," *Jurnal Ilmiah Teknik Elektro Komputer dan Informatika*, vol. 10, no. 4, pp. 665-680, 2024, https://doi.org/10.26555/jiteki.v10i4.29300.

[34] R. M. Naji, H. Dulaimi and H. Al-Khazraji, "An Optimized PID Controller Using Enhanced Bat Algorithm in Drilling Processes," *Journal Européen des Systèmes Automatisés*, vol. 57, no. 3, pp. 767-772, 2024, https://doi.org/10.18280/jesa.570314.

[35] M. A. Shaheen, H. M. Hasanien, S. F. Mekhamer, and H. E. Talaat, "Walrus optimizer-based optimal fractional order PID control for performance enhancement of offshore wind farms," *Scientific Reports*, vol. 14, no. 1, p. 17636, 2024, https://doi.org/10.1038/s41598-024-67581-x.

[36] A. K. Ahmed, H. Al-Khazraji, and S. M. Raafat, "Optimized PI-PD control for varying time delay systems based on modified Smith predictor," *International Journal of Intelligent Engineering & Systems*, vol. 17, no. 1, pp. 331-342, 2024, https://doi.org/10.22266/ijies2024.0229.30.

[37] P. Chotikunnan *et al*., "Genetic Algorithm-Optimized LQR for Enhanced Stability in Self-Balancing Wheelchair Systems," *Control Systems and Optimization Letters*, vol. 2, no. 3, 327-335, 2024, https://doi.org/10.59247/csol.v2i3.161.

[38] F. R. Yaseen and H. Al-Khazraji, "Optimized Vector Control Using Swarm Bipolar Algorithm for Five-Level PWM Inverter-Fed Three-Phase Induction Motor," *International Journal of Robotics and Control Systems*, vol. 5, no. 1, pp. 333-347, 2025, https://doi.org/10.31763/ijrcs.v5i1.1713.

[39] S. M. Mahdi, A. I. Abdulkareem, and A. J. Humaidi, "Improved Tracking Accuracy of Par-4 Delta Parallel Robot Using Optimized FOPID Control with PSO Technique," *Journal of Robotics and Control (JRC)*, vol. 6, no. 4, pp. 1721-1728, 2025, https://doi.org/10.18196/jrc.v6i4.26607.

[40] H. Al-Khazraji, W. Guo and A. J. Humaidi, "Improved cuckoo search optimization for production inventory control systems," *Serbian Journal of Electrical Engineering*, vol. 21, no. 2, pp. 187-200, 2024, https://doi.org/10.2298/SJEE2402187A.

[41] Z. Jin, X. Sun, G. Lei, Y. Guo and J. Zhu, "Sliding Mode Direct Torque Control of SPMSMs Based on a Hybrid Wolf Optimization Algorithm," *IEEE Transactions on Industrial Electronics*, vol. 69, no. 5, pp. 4534-4544, 2022, https://doi.org/10.1109/TIE.2021.3080220.

[42] Z. N. Mahmood, H. Al-Khazraji, and S. M. Mahdi, "Adaptive control and enhanced algorithm for efficient drilling in composite materials," *Journal Européen des Systems Automatisés*, vol. 56, no. 3, p. 507, 2023, https://doi.org/10.18280/jesa.560319.

[43] H. Al-Khazraji, "Comparative study of whale optimization algorithm and flower pollination algorithm to solve workers assignment problem," *International Journal of Production Management and Engineering*, vol. 10, no. 1, pp. 91-98, 2022, https://doi.org/10.4995/ijpme.2022.16736.

[44] L. Bo *et al*., "Improved Q-Learning Algorithm Based on Flower Pollination Algorithm and Tabulation Method for Unmanned Aerial Vehicle Path Planning," *IEEE Access*, vol. 12, pp. 104429-104444, 2024, https://doi.org/10.1109/ACCESS.2024.3434621.

[45] X. S. Yang, "Flower pollination algorithm for global optimization," *Unconventional Computing and Natural Computation*, pp. 240-249, 2012, https://doi.org/10.1007/978-3-642-32894-7_27.

[46] R. Zaheer and H. Shaziya, "A Study of the Optimization Algorithms in Deep Learning," *2019 Third International Conference on Inventive Systems and Control (ICISC)*, pp. 536-539, 2019, https://doi.org/10.1109/ICISC44355.2019.9036442.

[47] M. A. E. Mohamed, K. Jagatheesan, and B. Anand, "Modern PID/FOPID controllers for frequency regulation of interconnected power system by considering different cost functions," *Scientific Reports*, vol. 13, no. 1, p. 14084, 2023, https://doi.org/10.1038/s41598-023-41024-5.

[48] F. R Yaseen, M. Q. Kadhim, H. Al-Khazraji and A. J. Humaidi, "Decentralized Control Design for Heating System in Multi-Zone Buildings Based on Whale Optimization Algorithm," *Journal Européen des Systèmes Automatisés*, vol. 57, no. 4, pp. 981-989, 2024, https://doi.org/10.18280/jesa.570406.

[49] S. Singh, V. P. Singh, A. Mathur, T. K. Bashishtha, S. Padmanaban, and T. Varshney, "Airport microgrid control using integral-of-absolute-error having high renewable penetration," *Scientific Reports*, vol. 15, no. 1, p. 23550, 2025, https://doi.org/10.1038/s41598-025-04820-9.

[50] H. Al-Khazraji, C. Cole and W. Guo, "Dynamics analysis of a production-inventory control system with two pipelines feedback," *Kybernetes*, vol. 46, no. 10, pp. 1632-1653, 2017, https://doi.org/10.1108/K-04-2017-0122.